



# LUND UNIVERSITY

## Quantum Mechanics/Molecular Mechanics Study of the Reaction Mechanism of Glyoxalase I

Jafari, Sonia; Ryde, Ulf; Fouda, Adam Emad Ahmed; Alavi, Fatemeh Sadat; Dong, Geng; Irani, Mehdi

*Published in:*  
Inorganic Chemistry

*DOI:*  
[10.1021/acs.inorgchem.9b03621](https://doi.org/10.1021/acs.inorgchem.9b03621)

2020

*Document Version:*  
Peer reviewed version (aka post-print)

[Link to publication](#)

*Citation for published version (APA):*

Jafari, S., Ryde, U., Fouda, A. E. A., Alavi, F. S., Dong, G., & Irani, M. (2020). Quantum Mechanics/Molecular Mechanics Study of the Reaction Mechanism of Glyoxalase I. *Inorganic Chemistry*, 59, 2594–2603. <https://doi.org/10.1021/acs.inorgchem.9b03621>

*Total number of authors:*  
6

### General rights

Unless other specific re-use rights are stated the following general rights apply:

Copyright and moral rights for the publications made accessible in the public portal are retained by the authors and/or other copyright owners and it is a condition of accessing publications that users recognise and abide by the legal requirements associated with these rights.

- Users may download and print one copy of any publication from the public portal for the purpose of private study or research.
- You may not further distribute the material or use it for any profit-making activity or commercial gain
- You may freely distribute the URL identifying the publication in the public portal

Read more about Creative commons licenses: <https://creativecommons.org/licenses/>

### Take down policy

If you believe that this document breaches copyright please contact us providing details, and we will remove access to the work immediately and investigate your claim.

LUND UNIVERSITY

PO Box 117  
221 00 Lund  
+46 46-222 00 00

# QM/MM Study of the Reaction Mechanism of Glyoxalase I

Sonia Jafari,<sup>1,2</sup> Ulf Ryde,<sup>2</sup> Adam Emad Ahmed Fouda,<sup>2,†</sup> Fatemeh Sadat Alavi,<sup>2,‡</sup> Geng Dong,<sup>2,§</sup> Mehdi Irani,<sup>1,\*</sup>

<sup>1</sup> *Department of Chemistry, University of Kurdistan, P.O. Box 66175-416, Sanandaj, Iran*

<sup>2</sup> *Department of Theoretical Chemistry, Lund University, P. O. Box 124, SE-221 00 Lund, Sweden*

\*Correspondence to Mehdi Irani, E-mail: m.irani@uok.ac.ir,

Tel: +98 – 9128018046, Fax: +98 – 8733624133

2020-05-03

---

<sup>†</sup> Current address: School of Chemistry, University of Nottingham, Nottingham, UK.

<sup>‡</sup> Current address: Department of Chemistry, Faculty of Sciences, Shahid Beheshti University, Evin, Tehran, Iran.

<sup>§</sup> Current address: Department of Chemistry, Renmin University of China, Beijing, 100872, China.

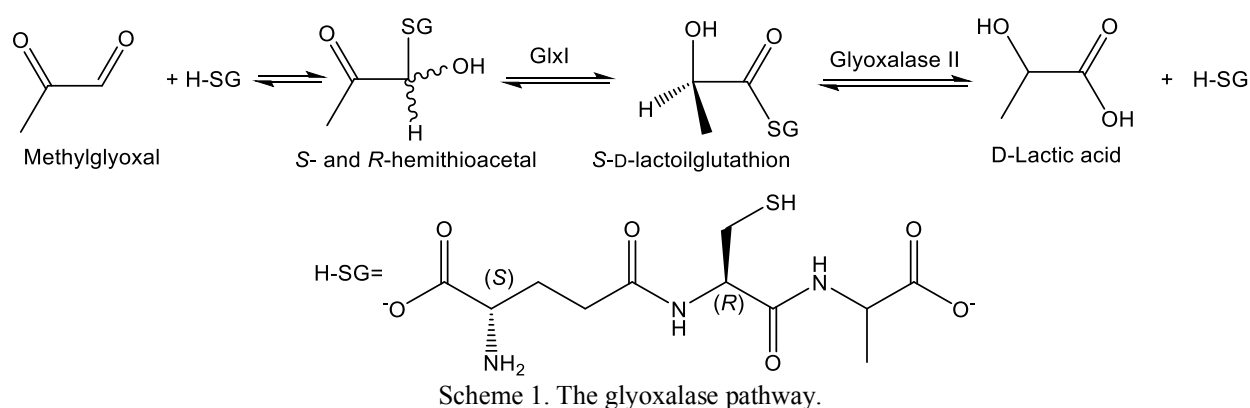
## Abstract

Glyoxalase I (GlxI) is a member of the glyoxalase system, which is important in cell detoxification and converts hemithioacetals of methylglyoxal (a cytotoxic byproduct of sugar metabolism that may react with DNA or proteins and introduce nucleic acid strand breaks, elevated mutation frequencies and structural or functional changes of the proteins) and glutathione into D-lactate. GlxI accepts both the *S* and *R* enantiomers of hemithioacetal, but converts them to only the *S*-D enantiomer of lactoylglutathione. Interestingly, the enzyme shows this unusual specificity with a rather symmetric active site (a Zn ion coordinated to two glutamate residues; Glu-99 and Glu-172), making the investigation of its reaction mechanism challenging. Herein, we have performed a series of combined quantum mechanics and molecular mechanics calculations to study the reaction mechanism of GlxI. The substrate can bind to the enzyme in two different modes, depending on the direction of its alcoholic proton (H2; toward Glu-99 or Glu-172). Our results show that the *S* substrate can react only if H2 is directed toward Glu-99 and the *R* substrate only if H2 is directed toward Glu-172. In both cases, the reactions lead to the experimentally observed *S*-D enantiomer of the product. In addition, the results do not show any low-energy paths to the wrong enantiomer of the product from neither the *S* nor the *R* substrate. Previous studies have presented several opposing mechanisms for the conversion of *R* and *S* enantiomers of the substrate to the correct enantiomer of the product. Our results confirm one of them for the *S* substrate, but propose a new one for the *R* substrate.

## 1. Introduction

Glyoxalase is a two-member enzymatic system with an unusual stereospecificity. It converts the *R*- and *S*-hemithioacetals of methylglyoxal (MG; a cytotoxic byproduct of sugar metabolism) and glutathione (H-SG) into D-lactate (cf. Scheme 1). The system is responsible for MG detoxification. MG may react with DNA or proteins and introduces nucleic acid strand breaks, elevated mutation frequencies,<sup>1,2</sup> or structural and functional changes of the proteins.<sup>3</sup>

The glyoxalase system was discovered in 1913.<sup>4-6</sup> In 1930s, it was shown that H-SG is a specific and essential cofactor for MG metabolism<sup>7</sup> and that H-SG and MG react reversibly to form a hemithioacetal substrate for the system.<sup>8</sup> In addition, in the same decade, it was found that the system converts the hemithioacetal into an acid-stable base-labile intermediate (nowadays known as *S*-D-lactoylglutathione).<sup>9</sup> In 1950s, Racker found that the system consists of two enzymes (glyoxalase I and II). The former catalyzes the formation of *S*-D-lactoylglutathione from hemithioacetal and the latter converts this intermediate to D-lactate<sup>10,11</sup> (cf. Scheme 1). The formation of D-lactate was later verified by Ekwall and Mannervik.<sup>12</sup> For a detailed historical survey of the system see reference<sup>13</sup>.



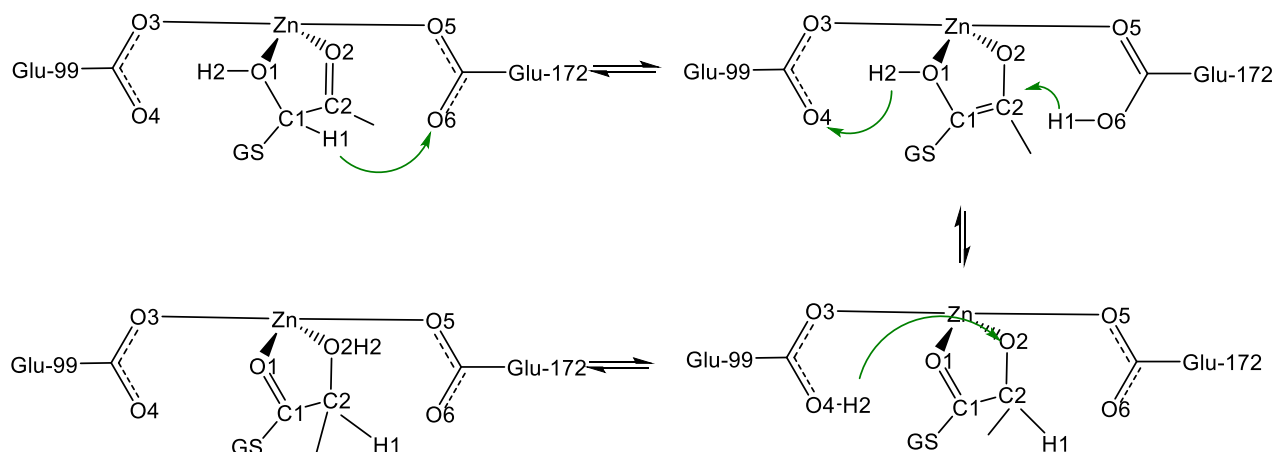
In this study we focus on the catalytic reaction of glyoxalase I (EC 4.4.1.5, lactoylglutathione lyase; GlxI). It converts both *R*- and *S*-hemithioacetals into the *S*-D enantiomer of lactoylglutathione<sup>4-12</sup> (the proper enantiomer of GlxI product; **DP**) but not into the *R*-L enantiomer (the wrong enantiomer of GlxI product; **LP**). Scheme 1 shows the complete glyoxalase pathway.

GlxI requires a divalent metal ion for its activity. The ion varies with the organism. It is Zn(II) for

the human<sup>14–16</sup> and yeast enzymes,<sup>17</sup> but Ni(II) for the *Escherichia coli*<sup>18,19</sup> and *Zea mays*<sup>20,21</sup> enzymes (the latter two proteins are inactive in presence of Zn(II) and have a reduced activity with the Co(II), Cd(II) and Mn(II) ions). The Zn ion of human GlxI is coordinated by His-126, Gln-33, Glu-99, Glu-172 and one or two water molecules in crystal structures of the resting enzyme.<sup>22,23</sup> The two active-site glutamate residues are coordinated symmetrically to the Zn ion (the Zn–OE1 distances are 2.04 and 1.97 Å or 1.98 and 2.02 Å, respectively).<sup>22</sup> When an inhibitor (*S*-[N-hydroxy-N-(p-iodophenyl)carbamoyl]glutathione; HIC-SG) binds to GlxI, it coordinates to the Zn ion, displacing the water molecules and detaching Glu-172 from the ion. This gives a penta-coordinated Zn site (1QIP pdb ID).<sup>23</sup> Thus, the symmetry of the Glu residues is broken in the HIC-SG-bound enzyme (the Zn–OE1 distances are 1.90 and 3.26 Å for Glu-99 and Glu-172, respectively). It was proposed that the displacement of Glu-172 gives it a higher basicity.<sup>23</sup> Recently, we confirmed the higher basicity of this residue by quantum mechanical cluster (QM-cluster) and hybrid quantum mechanics/molecular mechanics (QM/MM) calculations.<sup>24–26</sup> In addition, we showed through molecular dynamics (MD) simulations that Glu-172 has a higher flexibility than Glu-99 and this flexibility causes its displacement from the Zn ion and its higher basicity.<sup>25</sup> However, Hartree–Fock and density functional theory (DFT) calculations using relatively small models and symmetric glutamates could not explain the unusual specificity of GlxI.<sup>26–28</sup>

In the last two decades, different aspects of the catalytic mechanism of GlxI have been studied.<sup>22–</sup>  
<sup>37</sup> Two mechanisms were proposed for the reaction of the *S* substrate with GlxI in 2001.<sup>27–29</sup> Richter and Krauss (RK),<sup>28</sup> used Hartree–Fock calculations, coupled with a frozen effective fragment potential,<sup>38,39</sup> whereas Creighton and Hamilton (CH),<sup>29</sup> summarizing experimental aspects of the catalytic mechanism of GlxI up to that date, suggested independently the same three-step mechanism shown in Scheme 2. In the RK-CH mechanism, Glu-172 starts the reaction with abstraction of H1 from the substrate (see Scheme 2 for the naming of the atoms). Next, H1 is transferred from Glu-172 to C2 and H2 is concurrently transferred from O1 to Glu-99. Finally, O2 abstracts H2 from Glu-99, forming **DP**. In the same year, Himo and Siegbahn (HS) proposed a five-

step mechanism for the *S* substrate.<sup>27</sup> The first step is the same as for the RK-CH mechanism (abstraction of H1 by Glu-172), but the subsequent steps are different (the HS mechanism for the *S* substrate is shown in Scheme S1 and fully described in the Supporting Information).



Scheme 2. The RK-CH mechanism for the *S* substrate of GlxI. Note that the arrows in all schemes in this article indicate the movement of the protons, which gives a simpler view than the movement of electrons.

The most challenging part of the GlxI catalytic reaction is to explain how it accepts both enantiomers of its chiral substrate but converts them to the same enantiomer of the product and to describe the point where the two mechanisms join to form the same product. All previously proposed mechanisms for the *R* substrate suggest the same first step i.e. the abstraction of H1 by Glu-99,<sup>23,27–29</sup> but they suggest different steps for the subsequent reaction. RK<sup>28</sup> suggested that H2 is transferred to Glu172, whereas HS<sup>27</sup> proposed that H1 moves to O2. On the other hand, CH proposed that the enzyme first converts the *R* substrate to the *S* substrate (via dissociation of a glutathionyl mercaptide ion) and then processes the *S* substrate (the full proposed mechanisms for the *R* substrate by RK, HS and CH are shown in Schemes S2, S3 and S4 in the Supporting Information).

Recently, we have studied different aspects of the GlxI reaction in three separate works.<sup>24–26</sup> In the first work, we showed that the symmetric glutamates in a small QM-cluster model cannot reproduce the experimentally observed special stereospecificity of GlxI.<sup>26</sup> On the contrary, our results showed that with small QM-cluster models, like those used in previous studies,<sup>27,28</sup> the suggested mechanisms work equally well for the other enantiomer of the substrate, leading to the

incorrect enantiomer of the product. In the second work, we studied the catalytic reaction of a product analogue (glutathiohydroxyacetone), with the QM-cluster approach and MD simulations.<sup>25</sup> The results showed that an asymmetric QM-cluster model with a larger size for Glu-172, can reproduce the experimentally observed stereospecific proton exchange of the product analogue (a deuterium from the D<sub>2</sub>O medium can only be exchanged by the pro-*S* hydroxymethyl proton of the product analogue). Furthermore, MD simulations showed that Glu-172 is more flexible than Glu-99 in the crystal structure and is much closer to flexible loops inside the protein.<sup>25</sup> In our most recent work, using more accurate and expensive QM/MM calculations and free energy perturbations we studied the proton exchange reaction of a product analogue.<sup>24</sup> The results confirmed the proposed higher basicity of Glu-172. In summary, the three studies indicated that the higher basicity and flexibility of Glu-172 may explain the special stereospecificity of GlxI. Despite all previous studies,<sup>22–37</sup> there is not any computationally or experimentally confirmed mechanism for the reaction of the *R* enantiomer of the normal substrate of GlxI. Moreover, there are two opposing mechanisms for the *S* substrate and they are based on either a rather primitive *ab initio* method (HF/4-31G) or a small model of the active site with no constraints on the residues during optimization processes.<sup>27,28</sup> In addition, previous studies have not checked whether the suggested mechanisms also work on the other enantiomer of the substrate, giving the incorrect enantiomer of the product, i.e. they have not fully explained the intricate stereochemistry of GlxI.

In this study, QM/MM calculations with a large QM system (246 atoms) are employed to investigate the reactions of the *S* and *R* substrates of GlxI. Furthermore, we use the big-QM method<sup>40,41</sup> (single-point QM/MM calculations with 1336 atoms in the QM system) and QM/MM free energy perturbations<sup>42–44</sup> to obtain accurate energies. We scan all possible paths from all different binding modes of the substrates to find the most favorable paths for the reactions of the *S* and *R* substrates.

## 2. Methods

### 2.1 The Protein

All calculations are based on the 2.0 Å crystal structure of human GlxI (PDB code 1QIN).<sup>23</sup> The PDB structure contains a bound intermediate analogue (HIC-SG) in the active site, which mimics the binding of the substrate. Both subunits and all crystal-water molecules were included in the calculations. We built the substrate by modifying the HIC-SG molecule in one of the active sites. In the other active site, we replaced HIC-SG with two water molecules coordinated to the Zn ion. Thus, the reaction was assumed to take place in only one of the active sites, whilst the other site acted as a spectator. The same approach was successfully applied to other enzymatic systems.<sup>45,46</sup>

The protein setup was the same as in our previous studies of human GlxI.<sup>24,25</sup> The protonation states of all residues were determined by a study of the hydrogen-bond pattern, solvent accessibility and the possible formation of ionic pairs. They were also checked by PROPKA.<sup>47–49</sup> Details of the protonation states of all the protein residues are given in the Supporting Information. After assigning the protonation states, the protein was protonated and solvated with water molecules forming a sphere with a radius of 40 Å around the geometrical center of the protein, using the *leap* module of the Amber software package<sup>50</sup> (23,655 atoms in total). The added protons and water molecules were optimized by a 240 ps simulated annealing (up to 370 K) calculation, followed by a minimization, keeping the other atoms fixed at the crystal-structure positions. The protein, substrate and water molecules were described with the Amber99SB,<sup>51</sup> GAFF<sup>52</sup> force fields and the TIP3P model,<sup>53</sup> respectively. These calculations were performed using the AMBER program suite.<sup>50</sup>

### 2.2 QM/MM Calculations

The QM/MM calculations were performed with the ComQum software.<sup>54,55</sup> In this approach,<sup>56,57</sup> we split the protein and solvent into two subsystems: System 1 (the QM region) was treated by QM methods, System 2 (the MM region) contained the remaining part of the protein and solvent and was represented by an array of partial point charges, one for each atom, taken from MM libraries. It was kept fixed at the coordinates of the equilibrated protein. Junctions between systems 1 and 2



were treated with the hydrogen link-atom approach, as described in references 54 and 58. The QM calculations were performed at the TPSS-D3/def2-SV(P) level of theory,<sup>59–64</sup> using the Turbomole software<sup>65,66</sup> and was accelerated by the resolution-of-identity approximation.<sup>61,62</sup> In our previous studies on this enzyme with a rather small QM-cluster model, we used B3LYP functional, instead of TPSS.<sup>25,26</sup> Both are DFT methods, but the B3LYP calculations are more expensive and time consuming. Therefore, we used TPSS for the present QM/MM calculations with large QM systems. **xxx Again, i would be good if we can say that they give similar results.** The MM calculations were performed with the Amber software,<sup>50</sup> using the Amber ff14SB<sup>67</sup> and GAFF<sup>52</sup> force fields for the protein and the substrate, respectively. Water molecules were described by the TIP3P model.<sup>53</sup> Transition states were estimated from potential-energy scans of the corresponding reaction coordinate, which always was either an H–O or H–C distance. Further details of the ComQum calculations can be found in the Supporting information.

The QM system consisted of the Zn ion, Gln-33, His-126, Thr-97, Leu-98, Glu-99, Leu-100, Thr-101, Trp-170, Ile-171, Glu-172, Ile-173, Leu-174, HOC-SG and HOH-404 (the glutamine and histidine were included up to their alpha carbons, but all atoms of the other groups were included in the QM region; cf. Figure 1), giving a total of 246 atoms. We have also performed preliminary calculations with a smaller QM system (QM'; cf. Figure S1 in the Supporting Information). Calculations based on the QM' system gave similar reaction paths as those of the larger QM system. However, energies obtained with the larger QM system reproduced experimental data better. In the main paper, we report only results based on the larger QM system. Calculated reaction energy profiles based on the QM' system are shown in Figure S3 in the Supporting Information (using big-QM energies).

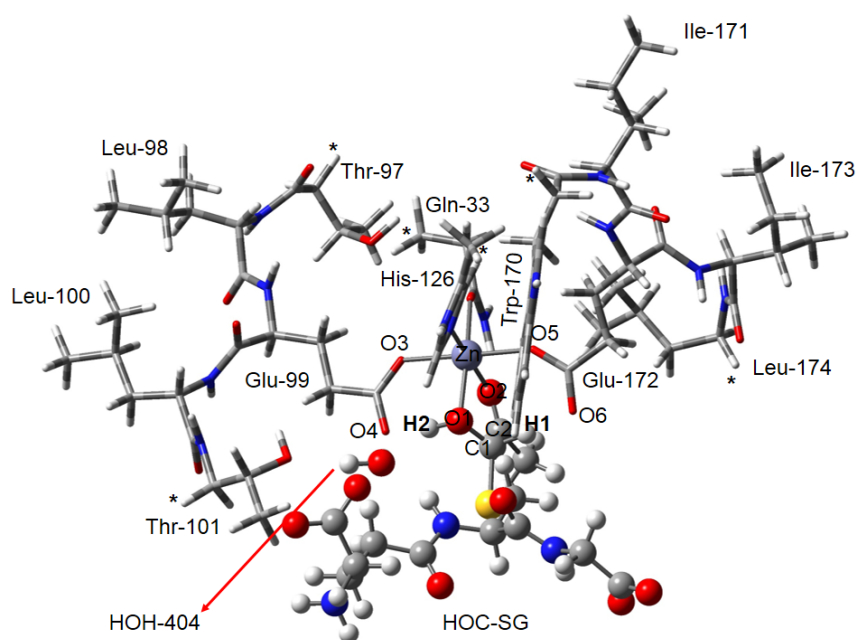


Figure 1. QM/MM structure of the **S1** state, showing the 246-atom QM system (see section 3 for definition of the states). The substrate, Zn ion and HOH-404 are shown in a ball-and-stick representation and the amino acids by tubes. Junction atoms are marked with asterisks.

## 2.3 Big-QM calculations

Previous studies have shown that QM/MM energies strongly depend on the size of the studied QM system.<sup>68,69</sup> Therefore, we have developed the big-QM approach to obtain converged QM/MM energies.<sup>40,41</sup> This method improves the QM/MM energies by choosing a very big QM system and moving junctions away from the reaction center.<sup>40</sup> In this work, the big-QM calculations include 1336 atoms in the QM region and 22,319 atoms in the MM system (cf. Figure S2 in the Supporting Information). The big-QM energy calculations were performed on the optimized QM/MM stationary structures as is described in the previous subsection, but they also employed the multipole-accelerated resolution-of-identity *J* approach (marij keyword).<sup>70</sup> We added the DFT-D3 dispersion correction and a standard MM correction ( $E_{\text{MM}12,q_1=0}^{\text{CL}} - E_{\text{MM}1,q_1=0}^{\text{HL}}$ ) to the big-QM energies, yielding a standard QM/MM energy but with the big-QM system as the QM region. Thus, both the QM/MM and big-QM calculations include the entire solvated protein, treated by standard MM methods (bonded, electrostatics and van der Waals terms). Further details of the big-QM calculations can be found in the Supporting information. Reported energies in the following are big-QM energies, except those in Figure 4, which also includes QTCP and QM/MM energies.

## 2.4 QTCP calculations

QM/MM thermodynamic cycle perturbation (QTCP) is a method to calculate free energies between two states, I and J, with a high-level QM/MM method, using free-energy perturbation with sampling only at the MM level.<sup>42–44</sup> It employs the thermodynamic cycle in Scheme S5 in the Supporting Information. The QTCP calculations were performed as has been described before.<sup>44,46</sup> Further details of the QTCP calculations can be found in the Supporting information and in <http://signe.teokem.lu.se/~ulf/Methods/qtcp.html>.

## 3. Results and Discussion

In this investigation, we perform an extensive and detailed QM/MM study on the reaction mechanism of GlxI. A primary problem with GlxI is the multitude of possible reaction paths. Here we attempt to systematically follow all possible paths. Both enantiomers of the substrate have been studied, differing at the C1 stereocenter (*S* or *R*). Moreover, each of them can bind to the enzyme in two different modes, depending on the direction of the H2 atom (pointing toward Glu-99 or Glu-172). These two modes cannot easily interconvert in the active site and give rise to different reaction paths.<sup>24,25</sup> Therefore, we have studied all possible reactions, starting from the four different starting structures. We call them **S1**, **S2**, **R1** and **R2**. The letter (in Italics) indicates the type of C1 stereocenter (*S* or *R*) and the number shows the direction of H2 (**1** indicates that H2 is directed toward Glu-99 and **2** indicates that H2 is directed toward Glu-172).

Figure 1 shows the QM/MM optimized structure of the **S1** state (the optimized structures of the other states are shown in Figure S4 in the Supporting Information and schematic views of all states are shown in Scheme 3). It can be seen that in the optimized structures of the **S2** and **R2** states, H2 is abstracted by Glu-172, whereas it remains bound to O1 in the **S1** and **R1** states. This confirms the higher basicity of Glu-172 compared to Glu-99, as was previously proposed.<sup>23–26</sup>

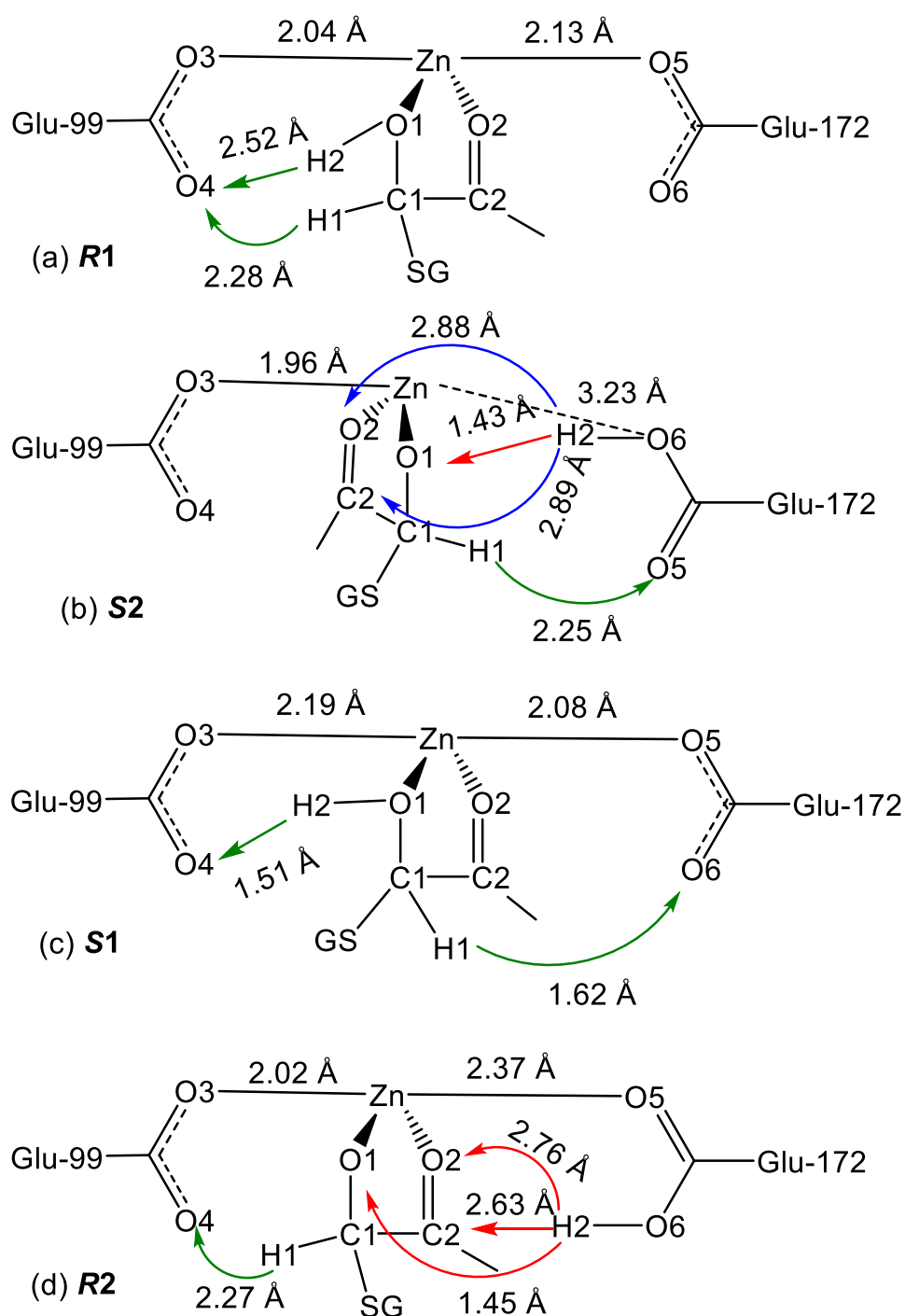
The big-QM energies of the four states are compared in Table 1, showing that the **S1**, **S2** and **R2**

states are almost degenerate, whereas the **R1** state is  $\sim 4$  kcal/mol less stable than the others. In the latter, both protons (H1 and H2) point toward Glu-99, which may destabilize it by steric effects. In the **S2** state both H1 and H2 are also on the same side (toward Glu-172). However, this is not reflected in the energies, because H2 is abstracted by Glu-172 in the **S2** state. Furthermore, the more basic and flexible Glu-172<sup>23–26</sup> is dissociated from the Zn ion in **S2** and reducing the steric crowding (the Zn–Glu-172 distance in **S2** is 3.23 Å, whereas the Zn–Glu-99 distance is 2.04 Å in **R1**; cf. Table S2 for more distances).

All possible reactions paths from the four states are shown in Scheme 3. Our calculations show that there is no path to any product from the states with H1 and H2 on the same side (the **R1** and **S2** states). However, there are possible reaction paths to the right enantiomer of the product from the states with H1 and H2 pointing in opposite directions (the **S1** and **R2** states). Therefore, we discuss the paths from the **S1** and **R2** states in the next two sections. Reactions from the **R1** and **S2** states are discussed in the Supporting Information.

Table 1. Big-QM energy differences between the **R2**, **R1**, **S1** and **S2** states.

State	Big-QM energy (kcal/mol)
<b>R2</b>	0.0
<b>R1</b>	3.9
<b>S1</b>	0.2
<b>S2</b>	0.5



**3.1 Scheme 3. Schematic views of the (a) *R1*, (b) *S2*, (c) *S1* and (d) *R2* states. The possible proton transfers are shown by arrows. Reaction paths from the *S1* state**

There are two possible proton transfers from ***S1***, H1 to Glu-172 and H2 to Glu-99 (cf. Scheme 3c). The results show that the H1 to O6 transfer (shown by a curved green arrow in Scheme 3c) is favorable with a barrier and a reaction energy of 3.8 and 1.1 kcal/mol, respectively (cf. Figure 2 for the energy profile). We call the product of this reaction ***S1-IM1*** (cf. Scheme 4a for the structure). There are three possible proton transfers from the ***S1-IM1*** state (shown in Scheme 4a). Our results

show that the transfers of H2 to Glu-99 or H1 to O2, shown by red arrows in Scheme 4a, are not possible (H1 and H2 returns to the starting point on Glu-172 and Glu-99 after releasing any constraints). On the other hand, the H1 to C2 transfer (shown by a green arrow in Scheme 4a) is possible with a barrier and reaction energy of 11.9 and  $-1.2$  kcal/mol, respectively. We name the resulting intermediate as **S1-IM2** and its schematic structure is shown in Scheme 4b. In **S1-IM2**, H2 is on Glu-99, making a close hydrogen bond to O2. It moved spontaneously from O1 to Glu-99 when transferring H1 to C2. From **S1-IM2**, there is only one reasonable proton transfer, H2 from Glu-99 to O2 (shown by a green arrow in Scheme 4b). This proton transfer has no barrier and produces the **DP** product (**S1-DP**; cf. Scheme 4c), which is almost degenerate with the reactant state (0.9 kcal/mol lower than **S1**; cf. Figure 2).

The second possible transfer from **S1** (H2 to Glu-99) is also favorable (the barrier and reaction energy are 3.0 and 2.0 kcal/mol, respectively) and produces **S1-IM1'** (cf. Scheme 4d for the structure). In fact, Glu-99 abstracts H2, but it forms a strong hydrogen bond to O1 (the H2–O4 and H2–O1 distances are 1.13 and 1.35 Å). From the **S1-IM1'** states there are three possible proton transfers (H1 to Glu-172 and H2 to C2 or O2). The results showed that the former produces the **S1-IM1** state (H2 returns to O1 when transferring H1 to Glu172) and the latter two transfers have very high barriers (56 and 41 kcal/mol for H2 to C2 and O2, respectively). Thus, there is only one feasible path from the **S1** state and it reaches to the proper enantiomer of the product (**S1**→**S1-IM1**→**S1-IM2**→**S1-DP**) with an overall reaction barrier of 14.0 kcal/mol.

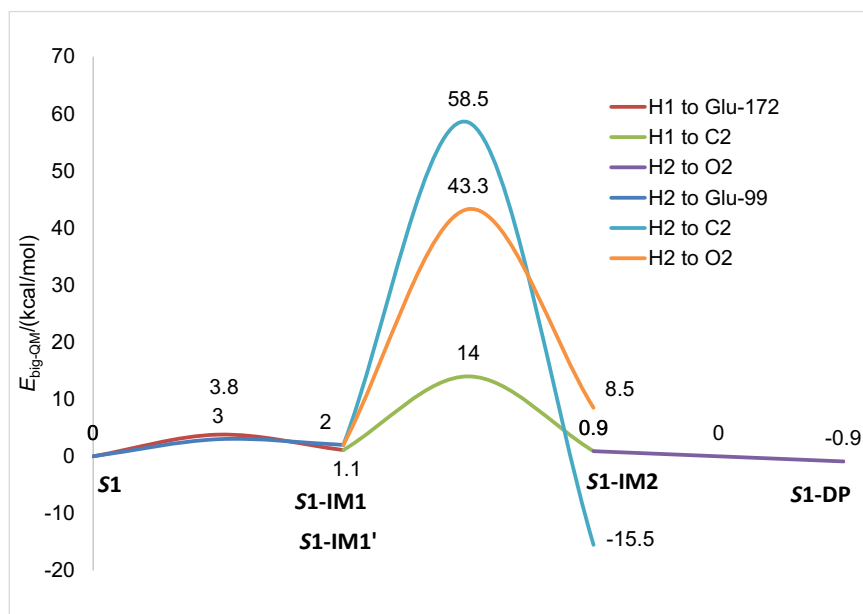
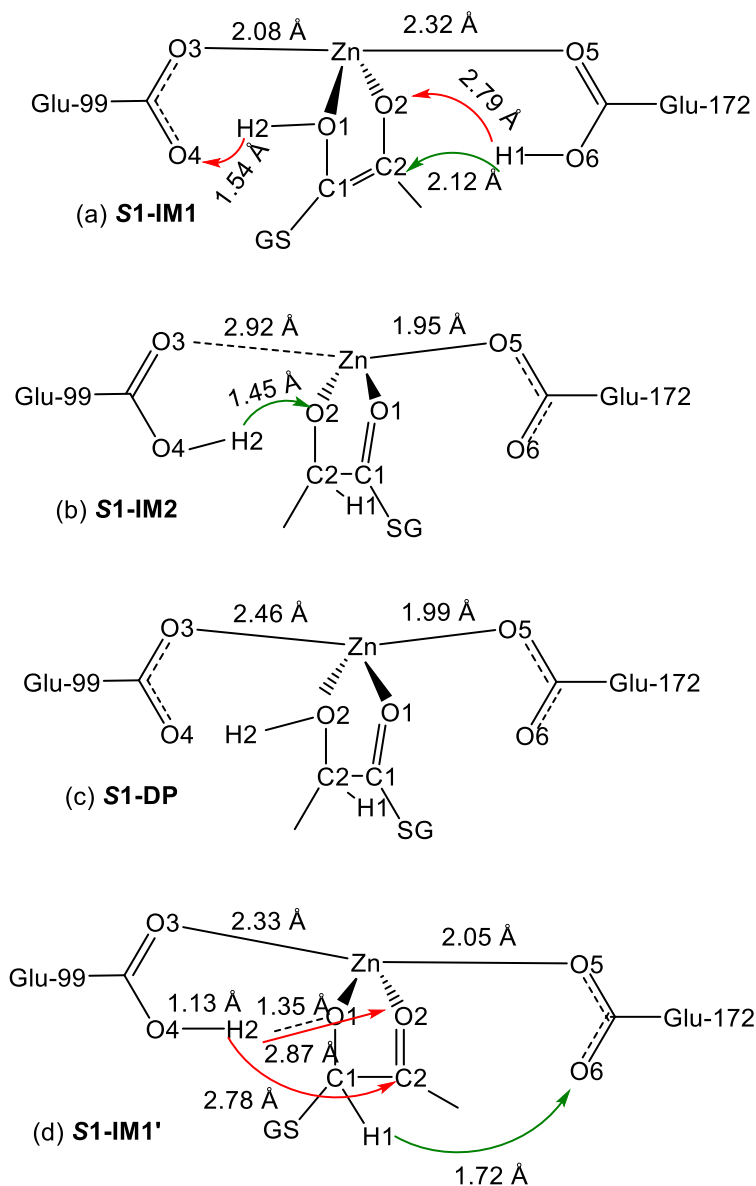


Figure 2. Energy profiles from the **S1** state.



Scheme 4. Schematic view and possible proton transfers of (a) **S1-IM1**, (b) **S1-IM2**, (c) **DP** from **S1**, **S1-DP** and (d) **S1-IM1'**.

### 3.2 Reaction paths from the **R2** state

Finally, we considered reaction paths starting from the **R2** state. There are four possible proton transfers from **R2** (shown by arrows in Scheme 3d). The results showed that the H2 to O2 transfer is not possible (it is strongly uphill and H2 returns on O6 after releasing the bond constraints, although the carboxyl group of Glu-172 rotates around the CG–CD bond to make a hydrogen bond with O2 instead of O1). Likewise, the H2 to C2 transfer has a high barrier (37 kcal/mol) and the H2 to O1 transfer is not possible. These three transfers are shown by red arrows in Scheme 3d. The reason for these unsuccessful transfers is that H2 is strongly sandwiched between O6 of Glu-172 and O1 in the **R2** state. This makes dissociation of H2 from Glu-172 energetically expensive. Furthermore, H2 is connected to the more basic Glu residue, making its dissociation less favorable.

On the other hand, our calculations showed that H1 can be transferred to Glu-99, producing **R2-IM1** (the barrier and reaction energy are 14.5 and 14.8 kcal/mol, respectively; cf. Figure 3). The formation of **R2-IM1** has a higher barrier and reaction energy than the formation of **S1-IM1** (3.8 and 1.1 kcal/mol, respectively). In **R2-IM1**, H2 is on Glu-172 and the substrate has lost two protons, giving a –2 charge on it, whereas the substrate has a single negative charge in **S1-IM1**, making its formation more favorable. This also confirms higher basicity of Glu-172.

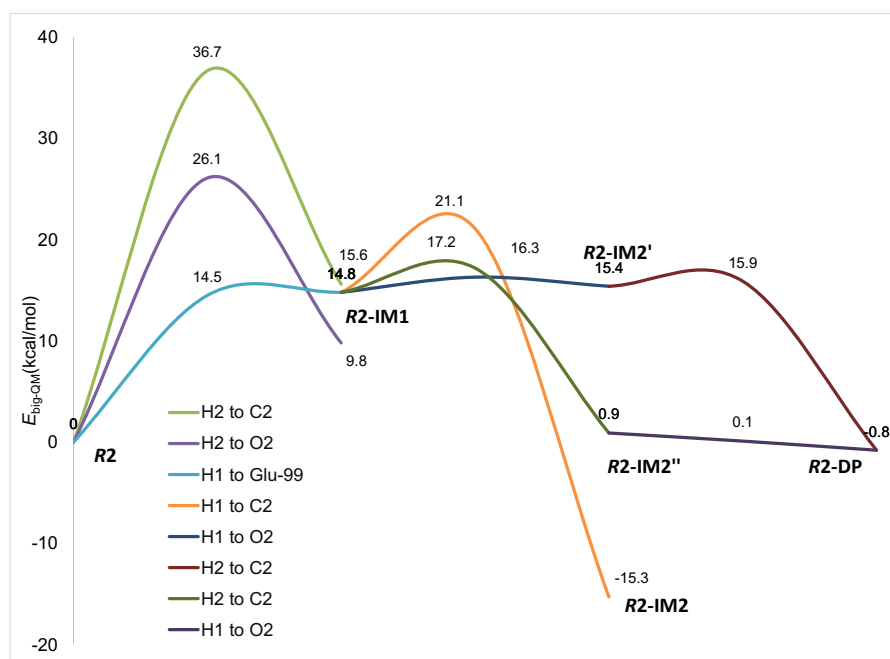


Figure 3. Energy profiles from the **R2** state.



Scheme 5. Schematic views and possible proton transfers of (a) **R2-IM1** (b) **R2-IM2** (c) **R2-IM2'** (d) **R2-DP** and (e) **R2-IM2''**.

From **R2-IM1**, there are four reasonable proton transfers (cf. Scheme 5a). The results show that the H2 to O2 proton transfer is not possible (it returns to the starting point after releasing any bond constraints) and the H1 to C2 proton transfer produces a very stable intermediate (**R2-IM2**; 15.3 kcal/mol more stable than **R2**). Production of **R2-IM2** could inhibit the enzyme, but the barrier for its production is quite high (21.1 kcal/mol). To produce a product from **R2-IM2**, H2 has to move from Glu-172 to O2 (cf. Scheme 5b). This would produce the incorrect enantiomer of the product. But the calculations showed that this transfer is not possible. Thus, there is no low-energy path to the incorrect enantiomer of the product from **R2**.

According to our results, the H1 to O2 proton transfer from **R2-IM1** crosses through a low barrier (1.5 kcal/mol) and reaches to the **R2-IM2'** intermediate, which is 15.4 kcal/mol higher than **R2** (cf. Figure 3). From **R2-IM2'** (Scheme 5c), H2 can be transferred to C2, via a low barrier (0.5 kcal/mol). This yields the proper enantiomer of the product (**R2-DP**; cf. Scheme 5d). The product is almost degenerate with the product of the **S1** state (**S1-DP**), although the H1 and H2 atoms are in opposite positions and point in different directions (compare Schemes 5d and 4c).

The H2 to C2 proton transfer from **R2-IM1** crosses through a low barrier 2.4 kcal/mol and reaches to **R2-IM2''** (cf. Scheme 5e). From **R2-IM2''**, the **DP** product can also be reached by transferring H1 to O2. Our results show that this transfer has no barrier. The barriers and reactions energies from the **R2** state are shown in Figure 3. The lowest overall barrier for production of **R2-DP** is 16.3 kcal/mol.

#### 4. Conclusions

Summing up the results (shown in Figures 2–4, S5 and S6), we have studied reactions starting from the four different substrate complexes (**R1**, **R2**, **S1** and **S2**). There is no path from the **R1** state

to any product. This state is also ~4 kcal/mol less stable than the other reactant states, because both H1 and H2 atoms point in the same direction, toward the less flexible and less basic Glu-99.

The **S2** state is 3.4 kcal/mol more stable than **R1**. Production of the wrong enantiomer of the product from this state is unlikely, because both H1 and H2 atoms point toward Glu-172, which in turn is on the *si* face side of C2. Abstraction of H1 by Glu-172 in **S2** is more favorable than abstraction of H1 by Glu-99 in **R1** (7.4 vs. 19.3 kcal/mol, compare the profiles in Figures S6 and S5). However, the produced intermediate in **S2** (**S2-IM1**) can pass only one proton to the substrate, producing either **S2-IM2** or **S2-IM2''**. These two states represent thermodynamic sinks which are 13.1 kcal/mol more stable than **S2**, and there is no path from them to the **DP** product. The **S2**→**S2-IM1**→**S2-IM2** path has a relatively low barrier (20.3 kcal/mol). However, there is a more favorable path from the **S1** binding mode to the product (**S1**→**S1-IM1'**→**S1-IM2**→**S1-DP**) with an overall barrier of 14.0 kcal/mol. This would make the former ~3600 times slower than the latter (using the Arrhenius equation at 300 K). Therefore, the path from the **S2** state to the thermodynamic sinks is unlikely.

In the **S1** binding mode, H2 is directed toward the Glu-99 residue and formation of the wrong enantiomer of the product could be conceivable (if Glu-99 abstracts H2 and pass it to the *re* face of C2). However, our results showed that Glu-99 can abstract H2 from the substrate, but cannot pass it to the *re* face of C2. Even after the first step (H1 to Glu-172), Glu-99 could not abstract H2, but H1 can be passed to C2, with a barrier of 14.0 kcal/mol. The reaction path from **S1** to **S1-DP** (**S1**→**S1-IM1**→**S1-IM2**→**S1-DP**) agrees with the path proposed by RK-CH<sup>28,29</sup> (cf. Scheme 2). On the other hand, our calculations do not support the HS mechanism<sup>27</sup> in Scheme S1 (H1 cannot move from Glu-172 to O2 in the second step from **S1-IM1**).

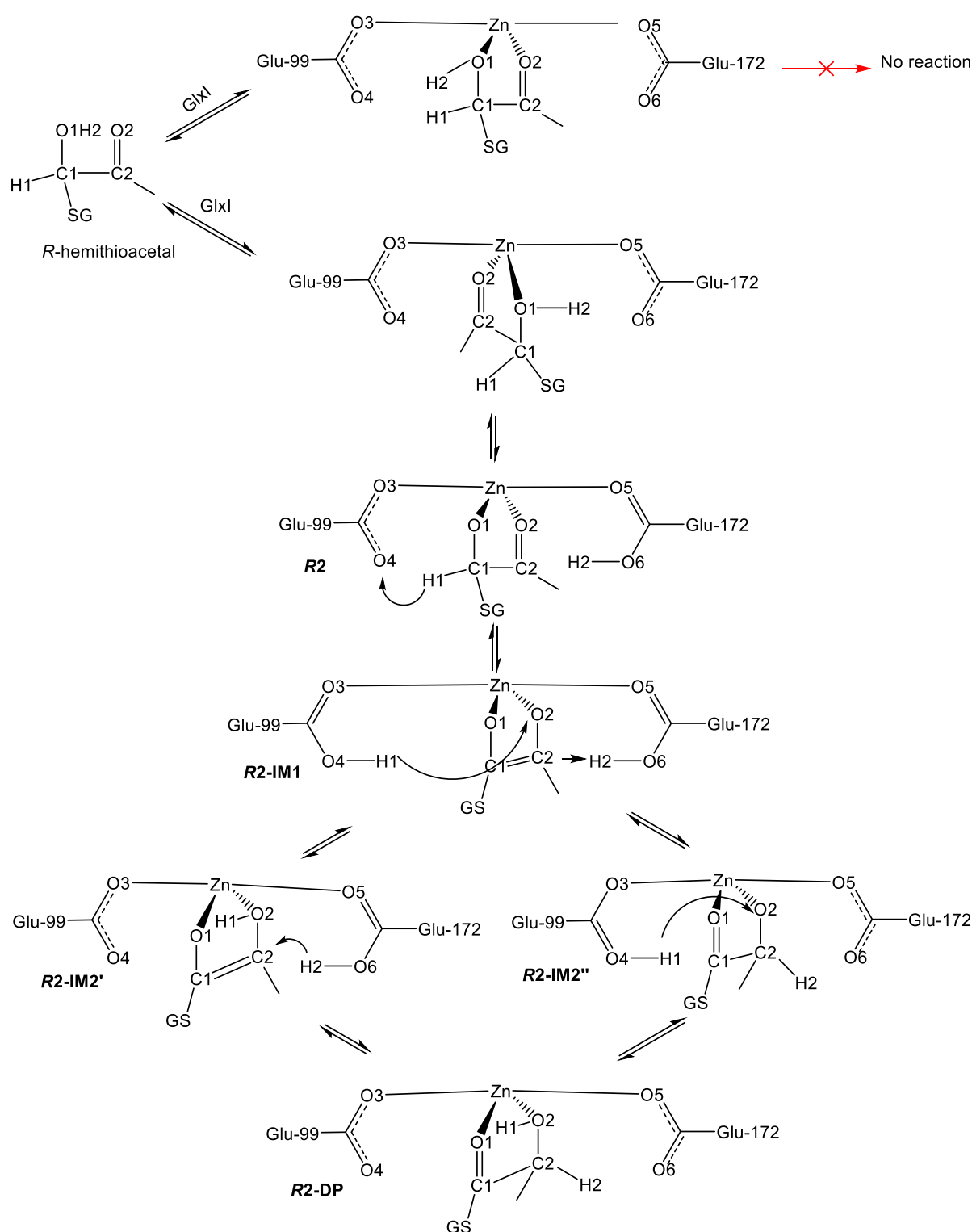
Our calculations show that the *R* substrate can bind in both the **R1** and **R2** modes. However, **R1** is 3.9 kcal/mol less stable than **R2** and there is no path from it to a product. From the **R2** state, H2 cannot accomplish any proton transfer in the first step. Therefore, Glu-99 must abstract H1, producing **R2-IM1**, and pass it to either the *re* face of C2, producing **R2-IM2**, or to O2 producing

**R2-IM2'**. The **R2-IM2** state could give rise to the wrong enantiomer of the product, but the last step is not possible (H2 to O2). Furthermore, the barrier of production of **R2-IM2** is 21.1 kcal/mol, making its production unlikely. On the other hand, our results show two alternative paths from **R2** to the **DP** product (**R2**→**R2-IM1**→ **R2-IM2'**→ **R2-DP** and **R2**→**R2-IM1**→ **R2-IM2''**→ **R2-DP**). Thus, based on the QM/MM calculations for the paths from the **R2** state, we propose the reaction mechanism for the *R*-substrate of GlxI in Scheme 6. It is the first computationally confirmed mechanism for the *R*-substrate. In our proposed mechanism, Glu-172 abstracts the alcoholic oxygen of the substrate (H2) upon binding. Then, Glu-99 abstracts H1 from C1. After that, the reaction can proceed by moving either H1 from Glu-99 to O2 or H2 from Glu-172 to C2. The results indicate that the two paths have similar barriers (16.3 and 17.2 kcal/mol). The first path produces **R2-IM2'** and the second path produces **R2-IM2''**. Finally, H2 can move from Glu-172 to O2 and H1 can move from Glu-99 to O2 in **R2-IM2'** and **R2-IM2''**, respectively, giving the **D** enantiomer of the product (**R2-DP**).

The second alternative path is almost the same mechanism proposed by RK for the *R* substrate (cf. Scheme S2). However, in our proposed path, H2 is abstracted by Glu-172 in the reactant state and not after abstraction of H1 by Glu-99 (compare mechanisms in Scheme S2 and Scheme 6). The QM/MM results indicate that the HS mechanism for the *R* substrate<sup>27</sup> (Scheme S3) is not possible, because structures with H1 on Glu-99 and H2 is directed toward Glu-172 are not stable (the first intermediate in the HS mechanism in Scheme S3). Instead, Glu-172 abstracts H2 in such a structure (**R2-IM1**; Scheme 5a). The reason for this discrepancy is most likely that HS used a very small QM-cluster model with 36 atoms and with no constraints on the terminal atoms of the amino acids and no model of the surroundings. This indicates that QM/MM calculations with big QM systems are needed to obtain accurate mechanism for challenging enzymatic systems like that of GlxI.

In conclusion, our results show that a proton can be abstracted from C1 of both enantiomers of the substrate, but it is always added to the *si* face of C2. This is in line with the results of Landro *et al.*,<sup>35</sup> which experimentally showed a non-stereospecific proton abstraction by the glutamates, but a

stereospecific proton delivery to the *si* face of C2 (the face which is directed to Glu-172).



Scheme 6. QM/MM based proposed mechanism for the conversion of *R*-hemithioacetal by GlxI.

To address the local-minima problem of the QM/MM calculations and to estimate also entropic effects, we recalculated the energy profiles for the three main reaction paths (*S1*→*S1-IM1*→*S1-IM2*→*S1-DP*, *R2*→*R2-IM1*→ *R2-IM2'*→ *R2-DP* and *R2*→*R2-IM1*→ *R2-IM2''*→ *R2-DP*) with

the QTCP method, which yields QM/MM free energies. These free-energy corrections were added to the big-QM energies according to  $E_{\text{tot}} = E_{\text{big-QM}} - E_{\text{QM/MM}} + \Delta G_{\text{QTCP}}$ . The results in Figure 4 show that the overall  $E_{\text{tot}}$  barriers for the reactions from the **S1** and **R2** states are 16.6 and 15.0 kcal/mol, respectively. These are in a reasonable agreement with the experimental reaction rate ( $k_{\text{cat}}=1500 \text{ s}^{-1}$ , corresponding to an activation barrier of  $\sim 14 \text{ kcal/mol}$ )<sup>71</sup> and the computationally calculated barriers (14.4 and  $\sim 13 \text{ kcal mol}^{-1}$  by HS and Åqvist *et al.*, respectively).<sup>27,36</sup> In addition, the  $E_{\text{tot}}$  energies show a lower barrier for the conversion of the *R* substrate compared to the conversion of the *S* substrate (15.0 kcal/mol vs. 16.6 kcal/mol). This is also in agreement with experiments which showed a faster conversion for the **R** enantiomer of glutathiolactaldehydes by GlxI (0.8 and  $0.4 \text{ s}^{-1}$  conversion rates for the **S** and **R** enantiomers of glutathiolactaldehydes, respectively).<sup>35</sup>

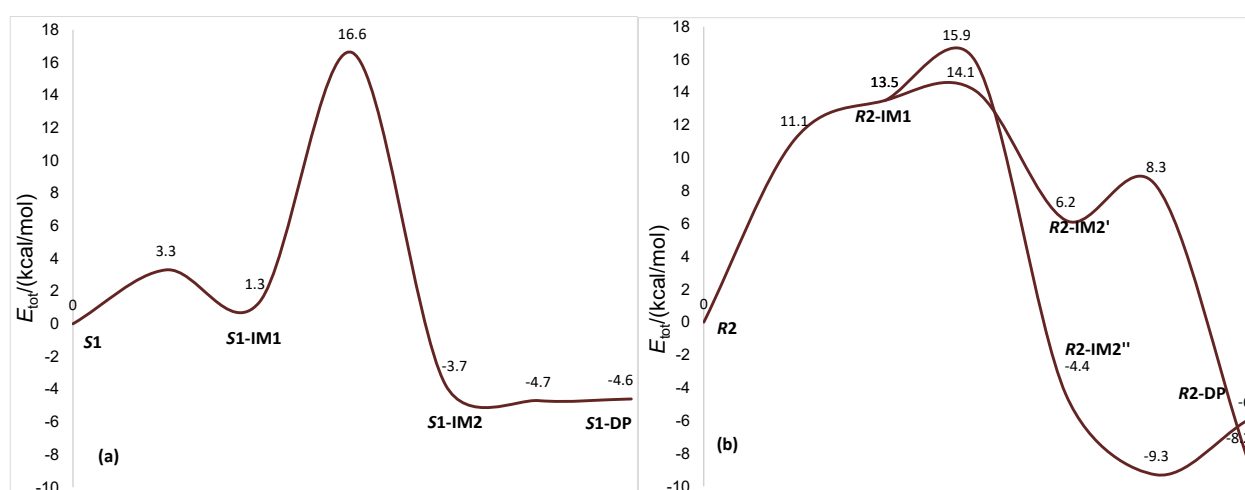


Figure 4. The  $E_{\text{tot}}$  energy profiles for the main path reactions (a) from the **S1** and (b) from the **R2** states. The energy component of  $E_{\text{tot}}$  is shown in Table S1 in the Supporting Information.

### Supporting Information Available:

The full description of the HS mechanism for the *S* substrate, schematic views for the *R* substrate by RK, HS and CH, details of the protonation states of the protein residues, details of the ComQum calculations, description of the QM' system and the corresponding energy profiles, details of the big-QM calculations, details of the QTCP calculations, optimized structures of **R1**, **R2** and **S2** states, results and discussion of the reactions from the **R1** and **S2** states, selected distances of the stationary structures, energy components of  $E_{\text{tot}}$  in Figure 4 and energy difference analysis between the stationary structures.

## Acknowledgements

This investigation has been supported by grants from the Swedish research council (project 2018-05003) and from the University of Kurdistan (project 4/7224). The computations were performed on computer resources provided by the Swedish National Infrastructure for Computing (SNIC) at Lunarc at Lund University and at HPC2N at Umeå University.

## 5. References

- (1) Lee, A. T.; Plump, A.; DeSimone, C.; Cerami, A.; Bucala, R. A Role for DNA Mutations in Diabetes-Associated Teratogenesis in Transgenic Embryos. *Diabetes* **1995**, *44* (1), 20–24. <https://doi.org/10.2337/diab.44.1.20>.
- (2) Murata-Kamiya, N.; Kamiya, H.; Kaji, H.; Kasai, H. Methylglyoxal Induces G:C to C:G and G:C to T:A Transversions in the SupF Gene on a Shuttle Vector Plasmid Replicated in Mammalian Cells. *Mutat. Res. - Genet. Toxicol. Environ. Mutagen.* **2000**, *468* (2), 173–182. [https://doi.org/10.1016/S1383-5718\(00\)00044-9](https://doi.org/10.1016/S1383-5718(00)00044-9).
- (3) Sibbersen, C.; Palmfeldt, J.; Hansen, J.; Gregersen, N.; Jørgensen, K. A.; Johannsen, M. Development of a Chemical Probe for Identifying Protein Targets of  $\alpha$ -Oxoaldehydes. *Chem. Commun.* **2013**, *49* (38), 4012–4014. <https://doi.org/10.1039/C3CC41099D>.
- (4) Neuberg, C. The Destruction of Lactic Aldehyde and Methylglyoxal by Animal Organs. *Biochem Z* **1913**, *49*, 502–506.
- (5) Neuberg, C.; Kerb, J. Über Zuckerfreie Hefegärungen. XII. Über Vorgänge Bei Der Hefegärung. *Biochem. Z* **1913**, *53*, 409–419.
- (6) Dakin, H. D.; Dudley, H. W. An Enzyme Concerned with the Formation of Hydroxy Acids from Ketonic Aldehydes. *J. Biol. Chem.* **1913**, *14* (2), 155–157.
- (7) Lohmann, K. A Study of the Enzymatic Transformation of Synthetic Methylglyoxal to Lactic

*Acid. Biochem. Z* **1932**, 254, 332–354.

- (8) Jowett, M.; Quastel, J. H. The Glyoxalase Activity of the Red Blood Cell: The Function of Glutathione. *Biochem. J.* **1933**, 27 (2), 486–498.
- (9) Yamazoye, S. Glyoxalase and Its Co-Enzyme: Iii. The Mechanism of the Action of Glutathione as the Co-Enzyme of Glyoxalase. *J. Biochem.* **1936**, 23 (2), 319–334. <https://doi.org/10.1093/oxfordjournals.jbchem.a125544>.
- (10) Racker, E. Glutathione as a Coenzyme in Intermediary Metabolism. *Glutathione* **1954**, 165–183. <https://doi.org/10.1016/B978-1-4832-2900-3.50020-1>.
- (11) Racker, E. The Mechanism of Action of Glyoxalase. *J. Biochem.* **1951**, 685–696.
- (12) Ekwall, K.; Mannervik, B. The Stereochemical Configuration of the Lactoyl Group of S-Lactoylglutathione Formed by the Action of Glyoxalase I from Porcine Erythrocytes and Yeast. *Biochim. Biophys. Acta - Gen. Subj.* **1973**, 297 (2), 297–299. [https://doi.org/10.1016/0304-4165\(73\)90076-7](https://doi.org/10.1016/0304-4165(73)90076-7).
- (13) Rabbani, N.; Thornalley, P. J. Glyoxalase Centennial Conference: Introduction, History of Research on the Glyoxalase System and Future Prospects. *Biochem. Soc. Trans.* **2014**, 42 (2), 413 LP – 418. <https://doi.org/10.1042/BST20140014>.
- (14) Ridderström, M.; Mannervik, B. Optimized Heterologous Expression of the Human Zinc Enzyme Glyoxalase I. *Biochem. J.* **1996**, 314 ( Pt 2 (Pt 2), 463–467. <https://doi.org/10.1042/bj3140463>.
- (15) Saint-Jean, A. P.; Phillips, K. R.; Creighton, D. J.; Stone, M. J. Active Monomeric and Dimeric Forms of Pseudomonas Putida Glyoxalase I: Evidence for 3D Domain Swapping. *Biochemistry* **1998**, 37 (29), 10345–10353. <https://doi.org/10.1021/bi980868q>.
- (16) Clugston, S. L.; Daub, E.; Kinach, R.; Miedema, D.; Barnard, J. F. J.; Honek, J. F. Isolation and Sequencing of a Gene Coding for Glyoxalase I Activity from Salmonella Typhimurium

and Comparison with Other Glyoxalase I Sequences. *Gene* **1997**, *186* (1), 103–111.  
[https://doi.org/10.1016/S0378-1119\(96\)00691-9](https://doi.org/10.1016/S0378-1119(96)00691-9).

- (17) Aronsson, A. C.; Marmstål, E.; Mannervik, B. Glyoxalase I, a Zinc Metalloenzyme of Mammals and Yeast. *Biochem. Biophys. Res. Commun.* **1978**, *81* (4), 1235–1240.  
[https://doi.org/10.1016/0006-291X\(78\)91268-8](https://doi.org/10.1016/0006-291X(78)91268-8).
- (18) Clugston, S. L.; Barnard, J. F. J.; Kinach, R.; Miedema, D.; Ruman, R.; Daub, E.; Honek, J. F. Overproduction and Characterization of a Dimeric Non-Zinc Glyoxalase I from Escherichia Coli: Evidence for Optimal Activation by Nickel Ions. *Biochemistry* **1998**, *37* (24), 8754–8763. <https://doi.org/10.1021/bi972791w>.
- (19) He, M. M.; Clugston, S. L.; Honek, J. F.; Matthews, B. W. Determination of the Structure of Escherichia Coli Glyoxalase I Suggests a Structural Basis for Differential Metal Activation. *Biochemistry* **2000**, *39* (30), 8719–8727. <https://doi.org/10.1021/bi000856g>.
- (20) González, J. M.; Agostini, R. B.; Alvarez, C. E.; Klinke, S.; Andreo, C. S.; Campos-Bermudez, V. A. Deciphering the Number and Location of Active Sites in the Monomeric Glyoxalase I of Zea Mays. *FEBS J.* **2019**, *286* (16), 3255–3271.  
<https://doi.org/10.1111/febs.14855>.
- (21) Turra, G. L.; Agostini, R. B.; Fauguel, C. M.; Presello, D. A.; Andreo, C. S.; González, J. M.; Campos-Bermudez, V. A. Structure of the Novel Monomeric Glyoxalase I from Zea Mays. *Acta Crystallogr. Sect. D Biol. Crystallogr.* **2015**, *71* (10), 2009–2020.  
<https://doi.org/10.1107/S1399004715015205>.
- (22) Cameron, A. D.; Olin, B.; Ridderström, M.; Mannervik, B.; Jones, T. A. Crystal Structure of Human Glyoxalase I - Evidence for Gene Duplication and 3D Domain Swapping. *EMBO J.* **1997**, *16* (12), 3386–3395. <https://doi.org/10.1093/emboj/16.12.3386>.
- (23) Cameron, A. D.; Ridderström, M.; Olin, B.; Kavarana, M. J.; Creighton, D. J.; Mannervik, B. Reaction Mechanism of Glyoxalase I Explored by an X-Ray Crystallographic Analysis of the



- Human Enzyme in Complex with a Transition State Analogue. *Biochemistry* **1999**, *38* (41), 13480–13490. <https://doi.org/10.1021/bi990696c>.
- (24) Jafari, S.; Ryde, U.; Irani, M. QM/MM Study of the Stereospecific Proton Exchange of Glutathiohydroxyacetone by Glyoxalase I. *Results Chem.* **2019**, *1*, 100011. <https://doi.org/10.1016/j.rechem.2019.100011>.
- (25) Jafari, S.; Kazemi, N.; Ryde, U.; Irani, M. Higher Flexibility of Glu-172 Explains the Unusual Stereospecificity of Glyoxalase I. *Inorg. Chem.* **2018**, *57* (9), 4944–4958. <https://doi.org/10.1021/acs.inorgchem.7b03215>.
- (26) Jafari, S.; Ryde, U.; Irani, M. Catalytic Mechanism of Human Glyoxalase I Studied by Quantum-Mechanical Cluster Calculations. *J. Mol. Catal. B Enzym.* **2016**, *131*, 18–30. <https://doi.org/10.1016/j.molcatb.2016.05.010>.
- (27) Himo, F.; Siegbahn, P. E. M. Catalytic Mechanism of Glyoxalase I: A Theoretical Study. *J. Am. Chem. Soc.* **2001**, *123* (42), 10280–10289. <https://doi.org/10.1021/ja010715h>.
- (28) Richter, U.; Krauss, M. Active Site Structure and Mechanism of Human Glyoxalase I-an Ab Initio Theoretical Study. *J. Am. Chem. Soc.* **2001**, *123* (19), 6973–6982. <https://doi.org/10.1021/ja0105966>.
- (29) Creighton, D. J.; Hamilton, D. S. Brief History of Glyoxalase I and What We Have Learned about Metal Ion-Dependent, Enzyme-Catalyzed Isomerizations. *Arch. Biochem. Biophys.* **2001**, *387* (1), 1–10. <https://doi.org/10.1006/abbi.2000.2253>.
- (30) Sousa Silva, M.; Ferreira, A. E. N.; Gomes, R.; Tomás, A. M.; Ponces Freire, A.; Cordeiro, C. The Glyoxalase Pathway in Protozoan Parasites. *Int. J. Med. Microbiol.* **2012**, *302* (4–5), 225–229. <https://doi.org/10.1016/j.ijmm.2012.07.005>.
- (31) Hall, S. S.; Doweyko, A. M.; Jordan, F. Glyoxalase I Enzyme Studies. 2. Nuclear Magnetic Resonance Evidence for an Enediol-Proton Transfer Mechanism. *J. Am. Chem. Soc.* **1976**, *98* (23), 7460–7461. <https://doi.org/10.1021/ja00439a077>.

- (32) Chari, R. V.; Kozarich, J. W. Deuterium Isotope Effects on the Product Partitioning of Fluoromethylglyoxal by Glyoxalase I. Proof of a Proton Transfer Mechanism. *J. Biol. Chem.* **1981**, *256* (19), 9785–9788.
- (33) Kozarich, J. W.; Chari, R. V. J. (Glutathiomethyl) Glyoxal: Mirror-Image Catalysis by Glyoxalase I. *J. Am. Chem. Soc.* **1982**, *104* (9), 2655–2657. <https://doi.org/10.1021/ja00373a062>.
- (34) Chari, R. V. J.; Kozarich, J. W. Glutathiohydroxyacetone: Proton NMR Determination of the Stereochemistry of Proton Exchange by Glyoxalase I. Evidence for a Cis-Enediol Intermediate Based on Mirror-Image Catalysis. *J. Am. Chem. Soc.* **1983**, *105* (24), 7169–7171. <https://doi.org/10.1021/ja00362a024>.
- (35) Landro, J. A.; Brush, E. J.; Kozarich, J. W. Isomerization of (R)- and (S)-Glutathiolactaldehydes by Glyoxalase I: The Case for Dichotomous Stereochemical Behavior in a Single Active Site. *Biochemistry* **1992**, *31* (26), 6069–6077. <https://doi.org/10.1021/bi00141a016>.
- (36) Feierberg, I.; Cameron, A. D.; Åqvist, J. Energetics of the Proposed Rate-Determining Step of the Glyoxalase I Reaction. *FEBS Lett.* **1999**, *453* (1–2), 90–94. [https://doi.org/10.1016/S0014-5793\(99\)00703-6](https://doi.org/10.1016/S0014-5793(99)00703-6).
- (37) Ridderström, M.; Cameron, A. D.; Jones, T. A.; Mannervik, B. Involvement of an Active-Site Zn<sup>2+</sup> Ligand in the Catalytic Mechanism of Human Glyoxalase I. *J. Biol. Chem.* **1998**, *273* (34), 21623–21628. <https://doi.org/10.1074/jbc.273.34.21623>.
- (38) Day, P. N.; Jensen, J. H.; Gordon, M. S.; Webb, S. P.; Stevens, W. J.; Krauss, M.; Garmer, D.; Basch, H.; Cohen, D. An Effective Fragment Method for Modeling Solvent Effects in Quantum Mechanical Calculations. *J. Chem. Phys.* **1996**, *105* (5), 1968–1986. <https://doi.org/10.1063/1.472045>.
- (39) Worthington, S. .; Krauss, M. Effective Fragment Potentials and the Enzyme Active Site.

- Comput. Chem.* **2000**, *24* (3–4), 275–285. [https://doi.org/10.1016/S0097-8485\(99\)00066-2](https://doi.org/10.1016/S0097-8485(99)00066-2).
- (40) Sumner, S.; Söderhjelm, P.; Ryde, U. Studies of Reaction Energies in Proteins. *J. Chem. Theory Comput.* **2013**, *9* (9), 4205–4214. <https://doi.org/dx.doi.org/10.1021/ct400339c>.
- (41) Hu, L.; Söderhjelm, P.; Ryde, U. Accurate Reaction Energies in Proteins Obtained by Combining QM/MM and Large QM Calculations. *J. Chem. Theory Comput.* **2013**, *9* (1), 640–649. <https://doi.org/10.1021/ct3005003>.
- (42) Luzhkov, V.; Warshel, A. Microscopic Models for Quantum Mechanical Calculations of Chemical Processes in Solutions: LD/AMPAC and SCAAS/AMPAC Calculations of Solvation Energies. *J. Comput. Chem.* **1992**, *13* (2), 199–213. <https://doi.org/10.1002/jcc.540130212>.
- (43) Rod, T. H.; Ryde, U. Quantum Mechanical Free Energy Barrier for an Enzymatic Reaction. *Phys. Rev. Lett.* **2005**, *94* (13), 138302. <https://doi.org/10.1103/PhysRevLett.94.138302>.
- (44) Rod, T. H.; Ryde, U. Accurate QM/MM Free Energy Calculations of Enzyme Reactions: Methylation by Catechol O-Methyltransferase. *J. Chem. Theory Comput.* **2005**, *1* (6), 1240–1251. <https://doi.org/10.1021/ct0501102>.
- (45) Srnec, M.; Aquilante, F.; Ryde, U.; Rulišek, L. Reaction Mechanism of Manganese Superoxide Dismutase Studied by Combined Quantum and Molecular Mechanical Calculations and Multiconfigurational Methods. *J. Phys. Chem. B* **2009**, *113* (17), 6074–6086. <https://doi.org/10.1021/jp810247u>.
- (46) Heimdal, J.; Kaukonen, M.; Srnec, M.; Rulišek, L.; Ryde, U. Reduction Potentials and Acidity Constants of Mn Superoxide Dismutase Calculated by QM/MM Free-Energy Methods. *ChemPhysChem* **2011**, *12* (17), 3337–3347. <https://doi.org/10.1002/cphc.201100339>.
- (47) Bas, D. C.; Rogers, D. M.; Jensen, J. H. Very Fast Prediction and Rationalization of PKa Values for Protein-Ligand Complexes. *Proteins Struct. Funct. Genet.* **2008**, *73* (3), 765–783.

<https://doi.org/10.1002/prot.22102>.

- (48) Olsson, M. H. M.; Søndergaard, C. R.; Rostkowski, M.; Jensen, J. H. PROPKA3: Consistent Treatment of Internal and Surface Residues in Empirical PK<sub>a</sub> Predictions. *J. Chem. Theory Comput.* **2011**, *7* (2), 525–537. <https://doi.org/10.1021/ct100578z>.
- (49) Jensen, J. H.; Li, H.; Robertson, A. D.; Molina, P. A. Prediction and Rationalization of Protein PK<sub>a</sub> Values Using QM and QM/MM Methods. *J. Phys. Chem. A* **2005**, *109* (30), 6634–6643. <https://doi.org/10.1021/jp051922x>.
- (50) Case, D. A.; Babin, V.; Berryman, J. T.; Betz, R. M.; Cai, Q.; Cerutti, D. S.; Cheatham, T. E.; Darden, T. A.; Duke, R. E.; Gohlke, H.; et al. Amber 14 - University of California: San Francisco, 2014.
- (51) Hornak, V.; Abel, R.; Okur, A.; Strockbine, B.; Roitberg, A.; Simmerling, C. Comparison of Multiple Amber Force Fields and Development of Improved Protein Backbone Parameters. *Proteins Struct. Funct. Bioinforma.* **2006**, *65* (3), 712–725. <https://doi.org/10.1002/prot.21123>.
- (52) Wang, J.; Wolf, R. M.; Caldwell, J. W.; Kollman, P. A.; Case, D. A. Development and Testing of a General Amber Force Field. *J. Comput. Chem.* **2004**, *25* (9), 1157–1174. <https://doi.org/10.1002/jcc.20035>.
- (53) Jorgensen, W. L.; Chandrasekhar, J.; Madura, J. D.; Impey, R. W.; Klein, M. L. Comparison of Simple Potential Functions for Simulating Liquid Water. *J. Chem. Phys.* **1983**, *79* (2), 926–935. <https://doi.org/10.1063/1.445869>.
- (54) Ryde, U. The Coordination of the Catalytic Zinc in Alcohol Dehydrogenase Studied by Combined Quantum-Chemical and Molecular Mechanics Calculations. *J. Comput. Aided. Mol. Des.* **1996**, *10* (2), 153–164. <https://doi.org/10.1007/BF00402823>.
- (55) Ryde, U.; Olsson, M. H. M. Structure, Strain, and Reorganization Energy of Blue Copper Models in the Protein. *Int. J. Quantum Chem.* **2001**, *81* (5), 335–347.

[https://doi.org/10.1002/1097-461X\(2001\)81:5<335::AID-QUA1003>3.0.CO;2-Q](https://doi.org/10.1002/1097-461X(2001)81:5<335::AID-QUA1003>3.0.CO;2-Q).

- (56) Ryde, U. QM/MM Calculations on Proteins. *Methods Enzymol.* **2016**, *577*, 119–158. <https://doi.org/10.1016/BS.MIE.2016.05.014>.
- (57) Senn, H. M.; Thiel, W. QM/MM Methods for Biomolecular Systems. *Angew. Chemie - Int. Ed.* **2009**, *48* (7), 1198–1229. <https://doi.org/10.1002/anie.200802019>.
- (58) Reuter, N.; Dejaegere, A.; Maigret, B.; Karplus, M. Frontier Bonds in QM/MM Methods: A Comparison of Different Approaches. *J. Phys. Chem. A* **2000**, *104* (8), 1720–1735. <https://doi.org/10.1021/jp9924124>.
- (59) Schäfer, A.; Horn, H.; Ahlrichs, R. Fully Optimized Contracted Gaussian-Basis Sets for Atoms Li to Kr. *J. Chem. Phys.* **1992**, *97* (4), 2571–2577. <https://doi.org/10.1063/1.463096>.
- (60) Tao, J.; Perdew, J. P.; Staroverov, V. N.; Scuseria, G. E. Climbing the Density Functional Ladder: Nonempirical Meta-Generalized Gradient Approximation Designed for Molecules and Solids. *Phys. Rev. Lett.* **2003**, *91* (14), 146401. <https://doi.org/10.1103/PhysRevLett.91.146401>.
- (61) Eichkorn, K.; Weigend, F.; Treutler, O.; Ahlrichs, R. Auxiliary Basis Sets for Main Row Atoms and Transition Metals and Their Use to Approximate Coulomb Potentials. *Theor. Chem. Accounts Theory, Comput. Model. (Theoretica Chim. Acta)* **1997**, *97* (1–4), 119–124. <https://doi.org/10.1007/s002140050244>.
- (62) Eichkorn, K.; Treutler, O.; Öhm, H.; Häser, M.; Ahlrichs, R. Auxiliary Basis Sets to Approximate Coulomb Potentials. *Chem. Phys. Lett.* **1995**, *240* (4), 283–289. [https://doi.org/10.1016/0009-2614\(95\)00621-A](https://doi.org/10.1016/0009-2614(95)00621-A).
- (63) Grimme, S.; Ehrlich, S.; Goerigk, L. Effect of the Damping Function in Dispersion Corrected Density Functional Theory. *J. Comput. Chem.* **2011**, *32* (7), 1456–1465. <https://doi.org/10.1002/jcc.21759>.

- (64) Grimme, S.; Antony, J.; Ehrlich, S.; Krieg, H. A Consistent and Accurate Ab Initio Parametrization of Density Functional Dispersion Correction (DFT-D) for the 94 Elements H-Pu. *J. Chem. Phys.* **2010**, *132* (15), 154104. <https://doi.org/10.1063/1.3382344>.
- (65) Von Arnim, M.; Ahlrichs, R. Performance of Parallel TURBOMOLE for Density Functional Calculations. *J. Comput. Chem.* **1998**, *19* (15), 1746–1757. [https://doi.org/10.1002/\(SICI\)1096-987X\(19981130\)19:15<1746::AID-JCC7>3.0.CO;2-N](https://doi.org/10.1002/(SICI)1096-987X(19981130)19:15<1746::AID-JCC7>3.0.CO;2-N).
- (66) Furche, F.; Ahlrichs, R.; Hättig, C.; Klopper, W.; Sierka, M.; Weigend, F. Turbomole. *Wiley Interdiscip. Rev. Comput. Mol. Sci.* **2014**, *4* (2), 91–100. <https://doi.org/10.1002/wcms.1162>.
- (67) Maier, J. A.; Martinez, C.; Kasavajhala, K.; Wickstrom, L.; Hauser, K. E.; Simmerling, C. Ff14SB: Improving the Accuracy of Protein Side Chain and Backbone Parameters from Ff99SB. *J. Chem. Theory Comput.* **2015**, *11* (8), 3696–3713. <https://doi.org/10.1021/acs.jctc.5b00255>.
- (68) Hu, L.; Eliasson, J.; Heimdal, J.; Ryde, U. Do Quantum Mechanical Energies Calculated for Small Models of Protein-Active Sites Converge? *J. Phys. Chem. A* **2009**, *113* (43), 11793–11800. <https://doi.org/10.1021/jp9029024>.
- (69) Hu, L.; Söderhjelm, P.; Ryde, U. On the Convergence of QM/MM Energies. *J. Chem. Theory Comput.* **2011**, *7* (3), 761–777. <https://doi.org/10.1021/ct100530r>.
- (70) Sierka, M.; Hogekamp, A.; Ahlrichs, R. Fast Evaluation of the Coulomb Potential for Electron Densities Using Multipole Accelerated Resolution of Identity Approximation. *J. Chem. Phys.* **2003**, *118* (20), 9136–9148. <https://doi.org/10.1063/1.1567253>.
- (71) Ridderström, M.; Cameron, A. D.; Jones, T. A.; Mannervik, B. Mutagenesis of Residue 157 in the Active Site of Human Glyoxalase I. *Biochem. J.* **1997**, *328* ( Pt 1 (1)), 231–235. <https://doi.org/10.1042/bj3280231>.



## TOC

### Synopsis:

QM/MM calculations show that the *S* substrate of glyoxalase I can react only if its alcoholic proton is directed toward Glu-99 and the *R* substrate only if the alcoholic proton is directed toward Glu-172 and both reactions lead to the experimentally observed *S*-D enantiomer of the product.